

Reentrant resistivity due to the interplay of superconductivity and magnetism in $\text{Eu}_{0.73}\text{Ca}_{0.27}(\text{Fe}_{0.87}\text{Co}_{0.13})_2\text{As}_2$

Lan Maria Tran ^{*}, Andrzej J. Zaleski , and Zbigniew Bukowski[†]*Institute of Low Temperature and Structure Research, Polish Academy of Sciences, Okólna 2, 50-422 Wrocław, Poland*

(Received 2 September 2023; revised 14 November 2023; accepted 18 December 2023; published 12 January 2024)

By simultaneous Co and Ca doping we were able to obtain an EuFe_2As_2 -based compound with superconductivity appearing above the antiferromagnetic order of Eu^{2+} magnetic moments. However, as soon as the antiferromagnetic order appears, a reentrance behavior is observed—instead of zero resistivity and diamagnetic signal down to the temperature of 2 K. By investigating magnetization, ac susceptibility, and electrical transport properties of $\text{Eu}_{0.73}\text{Ca}_{0.27}(\text{Fe}_{0.87}\text{Co}_{0.13})_2\text{As}_2$, and comparing them to previously studied Mössbauer effect and neutron scattering measurements of this and similar compounds, an explanation of such behavior is proposed.

DOI: [10.1103/PhysRevB.109.014509](https://doi.org/10.1103/PhysRevB.109.014509)

I. INTRODUCTION

Understanding of the relationship between magnetism and superconductivity in high-temperature superconductors is one of the remaining problems of the solid state physics. While superconductivity and magnetism are considered antagonistic phenomena, on the contrary, there are several groups of materials exhibiting both properties simultaneously [1–16]. Among them, the iron based superconductors are an extraordinary group, where the magnetic order and superconductivity originate from the same (iron) sublattice.

It was shown that, by suppression of the spin density wave (SDW) order (associated with the magnetic order on the Fe sublattice), superconductivity in $M\text{Fe}_2\text{As}_2$ (where $M = \text{Ca}, \text{Ba}, \text{Sr}, \text{Eu}$) compounds can be achieved. This can be a result of partial chemical substitution at either the M [17–20], Fe [20–29] or As [30,31] sites.

Due to the presence of the localized magnetism of Eu^{2+} ions, we find the EuFe_2As_2 -based compounds as one of the most interesting among the iron-based pnictide superconductors. In our previous study we focused on the properties of either Co or Ca doped EuFe_2As_2 compounds [32–34]. Based on these and other literature results (see Ref. [35]) it can be concluded that by diluting Fe by Co the temperature of the spin density wave (T_{SDW}) order associated with the Fe sublattice can be decreased and simultaneously superconductivity induced. Such substitution did not change the temperature of antiferromagnetic ordering of magnetic moments of Eu^{2+} ions (T_{N}); however, as shown by Mössbauer and neutron spectroscopies, the type of magnetic order on the Eu-sublattice changes significantly with decreased Co concentration [25,36]. On the other hand, Eu by Ca substitution decreased T_{N} , however such systems are not superconducting under ambient pressure [37–41] and, while the magnetic order on Eu sublattice does not change compared to the EuFe_2As_2 parent compound, the magnetic order on the Fe sublattice is modified below T_{N} [34,42].

Nevertheless, we believed that in the case of already superconducting systems, superconductivity can be enhanced if the antiferromagnetic order associated with Eu can be weakened or destroyed. Thus, we expected that with additional Ca doping we can obtain a superconducting system with lower T_{N} and higher T_{c} compared to those investigated by us $\text{Eu}(\text{Fe}_{0.81}\text{Co}_{0.19})_2\text{As}_2$ [32,33], and possibly a system where superconductivity appears above Eu magnetic order. Therefore, this study focuses on the properties of a double-doped compound— $\text{Eu}_{0.73}\text{Ca}_{0.27}(\text{Fe}_{0.87}\text{Co}_{0.13})_2\text{As}_2$ —with both Fe and Eu sublattices diluted by nonmagnetic ions.

II. EXPERIMENT

The single crystals of $\text{Eu}_{0.73}\text{Ca}_{0.27}(\text{Fe}_{0.87}\text{Co}_{0.13})_2\text{As}_2$ were grown using the Sn-flux method. High purity elements Eu:Ca:Co:Fe:As:Sn in nominal ratios 0.6:0.4:0.5:1.6:2:30 were inserted in an alumina crucible placed in a quartz tube, then evacuated and flame sealed. The ampule was heated with an approximately 100 °C/h heating ratio up to 1100 °C and held at this temperature for about 10 h, to enable proper dissolving of the components. The crystals grew while the solution was cooled with 1–2 °C/h ratio down to 600 °C. At this stage the liquid tin was decanted from the crucible. The remaining Sn was dissolved using diluted hydrochloric acid.

The chemical composition of the grown single crystals was determined using EDS spectroscopy. The crystal structure and phase purity of the samples was characterized by powder x-ray diffraction (XRD) using X'Pert Pro powder diffractometer equipped with a linear PIXcel detector and $\text{CuK}\alpha$ radiation.

To determine the properties of $\text{Eu}_{0.73}\text{Ca}_{0.27}(\text{Fe}_{0.87}\text{Co}_{0.13})_2\text{As}_2$ we measured electric transport (resistivity, magnetoresistivity, and Hall effect), magnetization, and ac susceptibility in the 2–300 K temperature range and in external magnetic fields up to 9 T. Measurements were performed for fields applied parallel and perpendicular to the crystallographic c axis (except Hall effect measurements where fields were only applied parallel to the c axis).

^{*}Corresponding author: l.m.tran@intibs.pl[†]deceased.

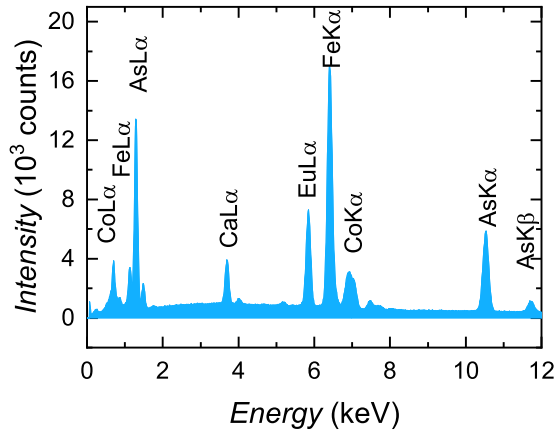


FIG. 1. EDX spectrum of $\text{Eu}_{0.73}\text{Ca}_{0.27}(\text{Fe}_{0.87}\text{Co}_{0.13})_2\text{As}_2$.

Electric transport and magnetization were investigated using Quantum Design's Physical Properties Measurement System (PPMS) platform. Resistivity (and magnetoresistivity) was measured using the four-point technique. Silver electrodes were attached to the sample's surface with DuPont silver paste. The measurements were carried out in fields both parallel and perpendicular to the c axis, while the ac electric current $I = 10$ mA with a frequency of 47 Hz was always applied parallel to the ab plane.

For Hall effect measurements two additional contacts were attached on the ab plane. To determine the Hall voltage U_H taking into account the error due to the misalignment of the Hall electrodes, the voltage on the Hall electrodes was measured while the sample was in magnetic field parallel and antiparallel to the c axis. The Hall voltage was then calculated as $U_H = (U_{H,180^\circ} - U_{H,0^\circ})/2$, where $U_{H,180^\circ}$ and $U_{H,0^\circ}$ are the voltage values measured while the sample was rotated by 180° and 0° , respectively.

The ac susceptibility was measured by applying a driving field of $\mu_0 H_{ac} = 10$ mT with a frequency of 1 kHz using the Oxford Susceptometer or the PPMS with the ACMS option.

In this contribution we present results obtained for one single crystal (unless stated otherwise), however all measurements were also performed for different crystals obtained from the same batch. Therefore, our conclusions are also based on the results obtained from these additional measurements. Chosen additional results are discussed in more detail in the Supplemental Material [43].

III. RESULTS

A. Composition and crystal structure

The EDX spectrum of one of the single crystal of $\text{Eu}_{0.73}\text{Ca}_{0.27}(\text{Fe}_{0.87}\text{Co}_{0.13})_2\text{As}_2$ is presented in Fig. 1. The composition of $\text{Eu}_{0.73}\text{Ca}_{0.27}(\text{Fe}_{0.87}\text{Co}_{0.13})_2\text{As}_2$ was determined by taking the average from measurements performed for several samples from the same batch. No traces of tin were detected.

Several crystals of $\text{Eu}_{0.73}\text{Ca}_{0.27}(\text{Fe}_{0.87}\text{Co}_{0.13})_2\text{As}_2$ from the same batch were ground to perform room temperature x-ray powder diffraction measurements. The collected diffraction pattern is presented in Fig. 2. All the observed reflections for

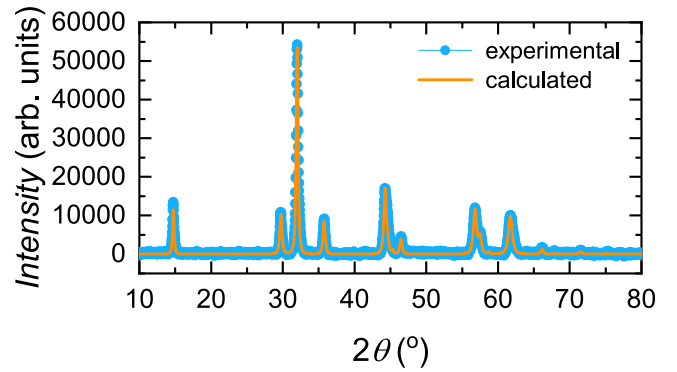


FIG. 2. Experimental (blue open circles) and calculated (solid orange lines) room-temperature XRD pattern of powdered crystals of $\text{Eu}_{0.73}\text{Ca}_{0.27}(\text{Fe}_{0.87}\text{Co}_{0.13})_2\text{As}_2$.

the investigated material could be indexed to the tetragonal ThCr_2Si_2 -type structure ($I4/mmm$ space group) expected for the AFe_2As_2 -based systems at room temperature. The refined lattice parameters are $a = 3.9075$ Å and $c = 12.0092$ Å. All reflexes could be indexed to the $I4/mmm$ space group, no foreign phases were detected.

B. Electric transport

1. Resistivity and magnetoresistivity

Temperature dependence of (zero-magnetic-field) resistivity normalized to resistivity at 300 K $\rho/\rho_{300\text{K}}(T)$ of $\text{Eu}_{0.73}\text{Ca}_{0.27}(\text{Fe}_{0.87}\text{Co}_{0.13})_2\text{As}_2$ is presented in Fig. 3, and a closeup of the 2–16 K temperature range is shown in the inset.

In the high temperature region, resistivity has a linear temperature dependence, down to about 80 K where the slope changes (see Fig. 3). High temperature anomalies of the resistivity dependence of the 122 systems are usually associated with the SDW ordering of the Fe 3d electrons [24,25] and, as was shown by the Mössbauer spectroscopy study, such is the case in the investigated compound [44].

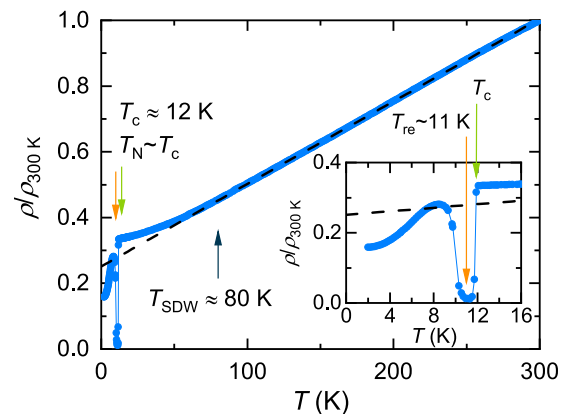


FIG. 3. Temperature dependence of resistivity normalized to the resistivity at 300 K of $\text{Eu}_{0.73}\text{Ca}_{0.27}(\text{Fe}_{0.87}\text{Co}_{0.13})_2\text{As}_2$; the inset presents normalized resistivity in the 2–16 K temperature range. The dashed line is the linear extrapolation of the data at temperatures above T_{SDW} .

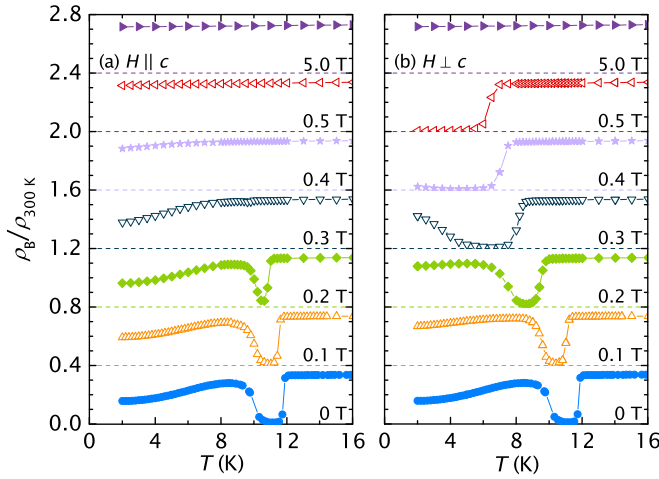


FIG. 4. Temperature dependence of magnetoresistivity normalized to $\rho_{300\text{K}}$ measured in external magnetic fields applied (a) parallel and (b) perpendicular to the c axis; note that the dependencies are artificially shifted along the y axis by 0.1 with the $\rho = 0$ level marked with dashed lines.

However, the most interesting behavior is observed below ~ 12 K, where the resistivity first rapidly decreases (due to the superconducting transition) and just before zero resistivity is reached, a reentrance of resistivity is observed, i.e., the resistivity increases with decreasing temperature and a resistive state is re-established.

Measurements carried out in external magnetic fields (see Fig. 4) reveal that the drop of resistivity as well as the reentrance are shifted to lower temperatures with increasing magnetic fields. However, depending on the direction of the applied field, the temperature dependencies are different. For fields applied parallel to the c axis, the drop of resistivity is smaller in each field and finally cannot be distinguished above fields of 0.3 T. On the other hand, for fields perpendicular to the c axis, the drop can be clearly observed and the superconducting transition is observed up to 3.5 T, while the “regrowth” is not visible at fields above 0.4 T in the investigated temperature range. Our explanation of this behavior is presented in Sec. IV.

Moreover, it should be noted that resistivity values below the “regrowth” are smaller than values expected from extrapolation of normal resistivity above 12 K (cf. dashed line in inset of Fig. 3).

From resistivity (magnetoresistivity) measurements, onset of the superconducting transition was determined as the temperature at which the resistivity starts to decrease rapidly, the data points are presented on Fig. 11 with solid blue stars [T_c - SC onset in $\rho_B(T)$]. In the same figure with blue open stars [$T_{\text{reentrance}}$ in $\rho_B(T)$] are presented data points corresponding to the temperatures at which the resistivity “regrows.”

2. Hall effect

Hall effect measurements were carried out in fields of 5 and 9 T, the respective temperature dependencies are presented in Fig. 5(a). Similarly, as was observed for other EuFe_2As_2 -based Co-doped compounds [24], the Hall coefficient changes with temperature, i.e., at high temperatures R_H decreases with

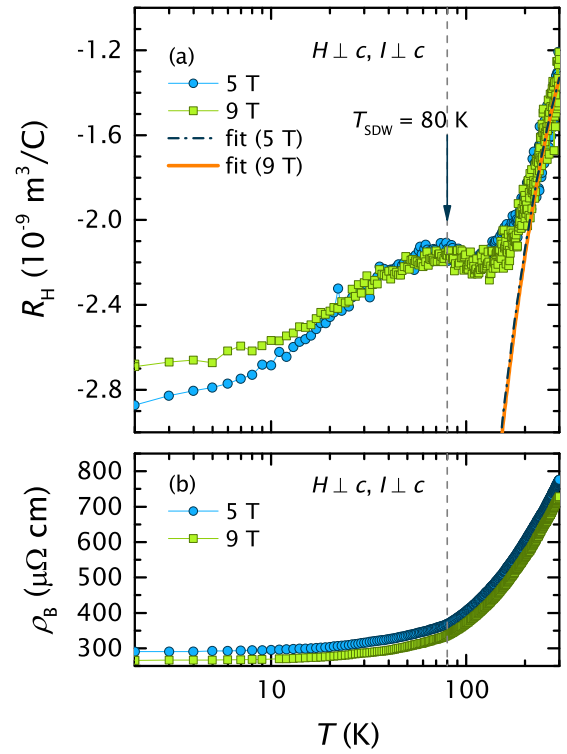


FIG. 5. Temperature dependence of (a) Hall coefficient R_H in 5 and 9 T with the fit of Eq. (1) and (b) magnetoresistivity at 9 T. The dashed line represents the SDW transition temperature.

decreasing temperature. While only a slight change of slope was detected in $\rho(T)$ and $\rho_B(T)$ at T_{SDW} [see Figs. 3 and 5(b)], a clear anomaly of the $R_H(T)$ is observed at this temperature [cf. Fig. 5(a)]. A similar anomaly near T_{SDW} was found in other EuFe_2As_2 -based Co-doped compounds [24,32,45].

In systems with spin-orbit interactions between the conducting electrons and localized moments, Hall coefficients consist of two components—the ordinary R_o and anomalous R_s contributions—and can be written as

$$R_H = R_o + R_s \chi_V(T), \quad (1)$$

where $\chi_V(T)$ is the temperature dependent volume susceptibility (in SI units) calculated from magnetization. The fitting of Eq. (1) to the experimental data in 250–300 K temperature range is presented as a solid line in Fig. 5. The best fitting parameters are $R_o = 3.18 \cdot 10^{-10} \text{ m}^3/\text{C}$ and $R_s = -3.30 \cdot 10^{-7} \text{ m}^3/\text{C}$ for the 5 T measurements, while $R_o = 3.74 \cdot 10^{-10} \text{ m}^3/\text{C}$ and $R_s = -3.42 \cdot 10^{-7} \text{ m}^3/\text{C}$ for the 9 T data. A high ratio R_s/R_o of order of 1000 suggests a dominance of the spin-orbit coupling in the high-temperature region.

The Hall coefficient is negative over all investigated temperature region, which suggests electrons as majority carriers in $\text{Eu}_{0.73}\text{Ca}_{0.27}(\text{Fe}_{0.87}\text{Co}_{0.13})_2\text{As}_2$. While it is known that iron based superconductors are multiband systems [35], with the provided data results it is not possible to separate the components associated with the hole and electron carriers and only a one-band model can be used. This enables crude estimation of the carrier concentration n and mobility μ_H of the system.

TABLE I. Ordinary and anomalous Hall coefficients, carrier concentration, and mobility determined from fitting of Eq. (1) to experimental data and calculated in the one-band model.

	5 T	9 T
R_o in m^3/c	$3.18 \cdot 10^{-10}$	$3.74 \cdot 10^{-10}$
R_s in m^3/c	$-3.30 \cdot 10^{-7}$	$-3.42 \cdot 10^{-7}$
n in $1/m^3$	$1.96 \cdot 10^{28}$	$1.67 \cdot 10^{28}$
μ_H in $cm^2/V \cdot s$	0.41	0.51

In this model, the carrier concentration equals

$$n = \frac{1}{e_0 R_o}, \quad (2)$$

where $e_0 = 1.6 \cdot 10^{-19}$ C is the value of elementary electric charge, while carrier mobility equals

$$\mu_H = |R_o| \sigma = \frac{|R_o|}{\rho}, \quad (3)$$

where carrier conductivity σ is defined as inverse resistivity $1/\rho$. The calculated parameters for $\text{Eu}_{0.73}\text{Ca}_{0.27}(\text{Fe}_{0.87}\text{Co}_{0.13})_2\text{As}_2$ are summarized in Table I.

Similar results were obtained for other Co-doped EuFe_2As_2 -based compounds [24,32].

C. Magnetization

Field dependent magnetization measured in several temperatures is presented in Fig. 6. No spontaneous magnetization was detected, and the initial magnetization increases linearly with increasing external magnetic field, which is expected for an AF-system. All magnetization curves saturate above a certain magnetic field. The saturation magnetization for the 2 K measurement is around $\mu_{\text{sat}} \approx 7.05 \mu_B$, which is consistent with the theoretical value for Eu^{2+} ion $\mu_{\text{sat}}^{\text{theo}} = g \mathcal{J} \mu_B = 7 \mu_B$ (where $g = 2$ and $\mathcal{J} = 7/2$), indicating that all magnetic moments order ferromagnetically (field induced ferromagnetic order).

Depending on the direction of applied magnetic field, the initial slopes of $M(H)$ are distinctly different with a higher slope value for measurements performed in fields applied parallel to the c axis (cf. Fig. 7). The transition field between AF and field induced ferromagnetic orders H_{cr} can be determined

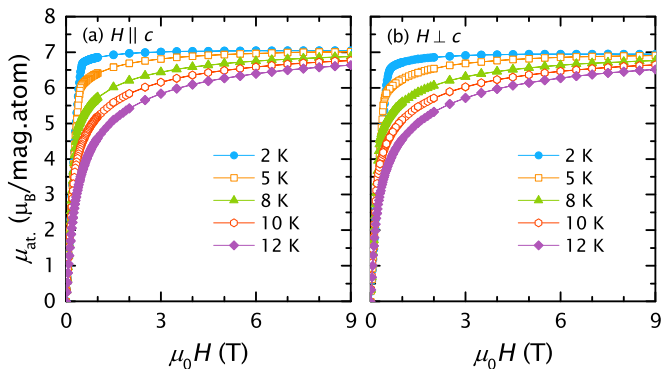


FIG. 6. Field dependent magnetization measured at magnetic fields applied (a) parallel and (b) perpendicular to the c axis.

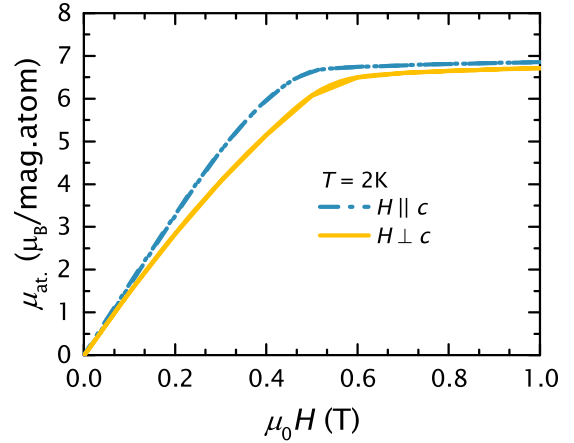


FIG. 7. Comparison of the initial slope of field dependent magnetization measured at 2 K while the magnetic field was applied parallel and perpendicular to the c axis.

by taking the minimum of the second derivative of magnetization d^2M/dH^2 . The calculated data points are collected on the magnetic phase diagram in Fig. 11 as orange squares.

Temperature dependence of inverted dc susceptibility investigated at 9 T is presented in Fig. 8. The dependence at high temperatures could be fitted using the modified Curie-Weiss

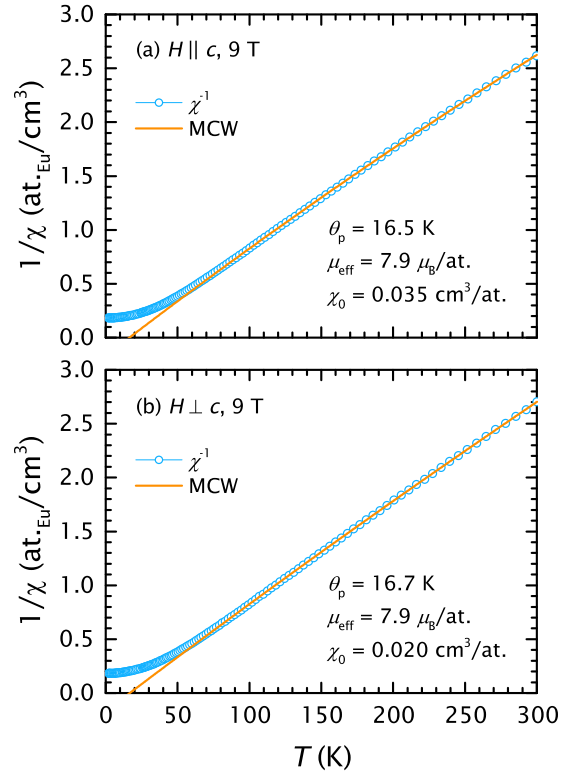


FIG. 8. Temperature dependence of inverted dc susceptibility measured in 9 T magnetic field applied (a) parallel and (b) perpendicular to the c axis; the solid line represents the fitting of Eq. (4) in the 100–300 K temperature range.

law

$$\chi(T) = \frac{N_A}{3k_B\mu_0} \frac{\mu_{\text{eff}}^2}{T - \theta_p} + \chi_0, \quad (4)$$

where N_A is the Avogadro's constant, k_B the Boltzmann's constant, μ_0 permeability of free space, θ_p the paramagnetic Curie temperature (or Weiss temperature), μ_{eff} effective magnetic moment (in Bohr magnetons μ_B), and χ_0 the temperature independent component of susceptibility. The fitting parameters are summarized in Fig. 8.

The evaluated effective magnetic moments per Eu atom μ_{eff} is equal to the theoretical value $\mu_{\text{eff}}^{\text{theo}} = g\sqrt{\mathcal{J}(\mathcal{J} + 1)} = 7.9 \mu_B$ for divalent Eu^{2+} ions. The constant χ_0 contribution is negligibly small when compared to the main magnetic susceptibility, confirming the absence of other phases.

While the Weiss temperature θ_p is positive, a ferromagnetic interaction is expected. However, as shown for EuCo_2As_2 [46] and multiple EuFe_2As_2 -based compounds [32,34,45,47–49], the Weiss temperature is positive although the system is antiferromagnetic. As discussed in Ref. [34], the sign of Weiss temperature is affiliated to the interactions between the nearest neighbors, therefore the positive value suggests a ferromagnetic interaction among nearest Eu^{2+} ions in the ab plane.

The Néel temperature was determined using the Fisher's method [50]. For fields applied parallel to the c axis, the maximum of $d\chi(T)T/dT$ was not certain, therefore the transition temperature was only estimated for this data set; the procedure where the data points were estimated is described in the Supplemental Material [43]. The evaluated data points are summarized on the magnetic phase diagram in Fig. 11 as orange triangles.

D. Susceptibility

The temperature dependence of ac susceptibility was measured in external magnetic fields applied either parallel or perpendicular to the c axis. The ac susceptibility measurements turned out to be a very sensitive technique, showing where most differences between individual crystals were observed. Nevertheless, the differences were in quantity not the quality of the results. In Fig. 9 we present ac susceptibility measured for several external magnetic fields applied parallel and perpendicular to the c axis. For comparison, in Fig. 10 zero field ac susceptibility measured for another crystal (from the same batch) is shown.

The temperature dependent real part of susceptibility $\chi'(T)$ measured at zero magnetic field exhibits a broad maximum at around 12 K (cf. Figs. 9 and 10, see also Ref. [43]).

For measurements with the driving field H_{ac} applied parallel to the c axis, at $T_c = 12$ K, $\chi'(T)$ decreases rapidly and for some samples adopts negative values for a narrow 1–2 K temperature range (cf. Fig. 10). At corresponding temperature the imaginary part of susceptibility $\chi''(T)$ has a sharp peak. Below 10 K, χ'' has another “peak,” however a very broad one. With application of an external magnetic field, both the dip in $\chi'(T)$ and the sharp peak in $\chi''(T)$ shift to the lower temperatures with increasing magnetic field; additionally, their intensities decrease and both the peak and the dip cannot be distinguished above 0.25 T. Additionally, two sep-

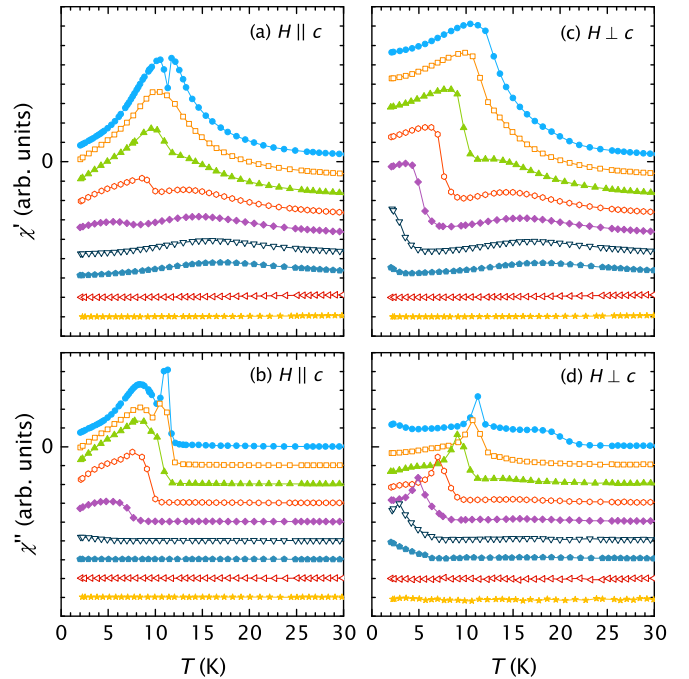


FIG. 9. Temperature dependencies of (a), (d) real χ' and (b), (d) imaginary χ'' parts of ac susceptibility investigated in (from top to bottom) 0, 0.1, 0.2, 0.3, 0.4, 0.5, 0.6, 5, and 9 T external magnetic fields applied (a), (b) parallel and (c), (d) perpendicular to the c axis measured using a driving field of 10 mT with a frequency 1000 Hz; data for subsequent fields are intentionally shifted along the y axis by -1 unit for better visibility.

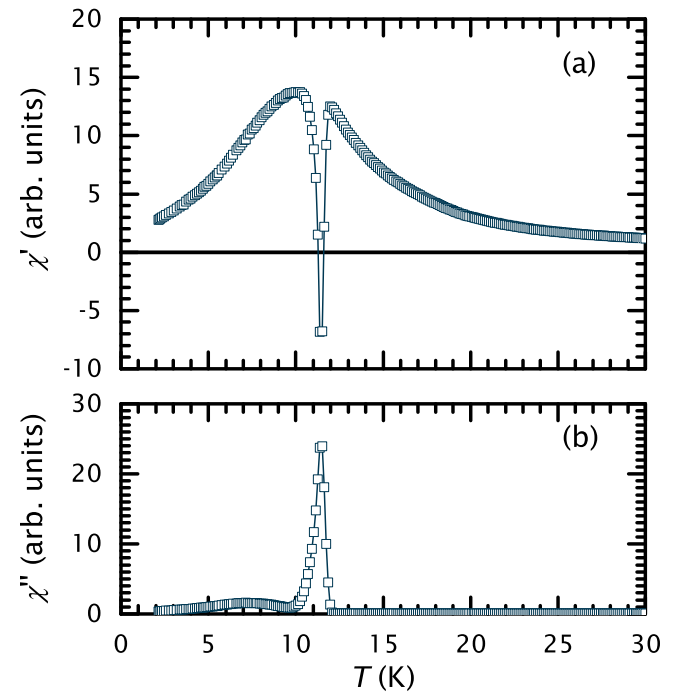


FIG. 10. Temperature dependence of (a) real χ' and (b) imaginary χ'' parts of ac susceptibility measured in zero external magnetic field using a driving field of 10 mT with a frequency of 1000 Hz applied parallel to the c axis for another crystal of $\text{Eu}_{0.73}\text{Ca}_{0.27}(\text{Fe}_{0.87}\text{Co}_{0.13})_2\text{As}_2$ obtained from the same batch.

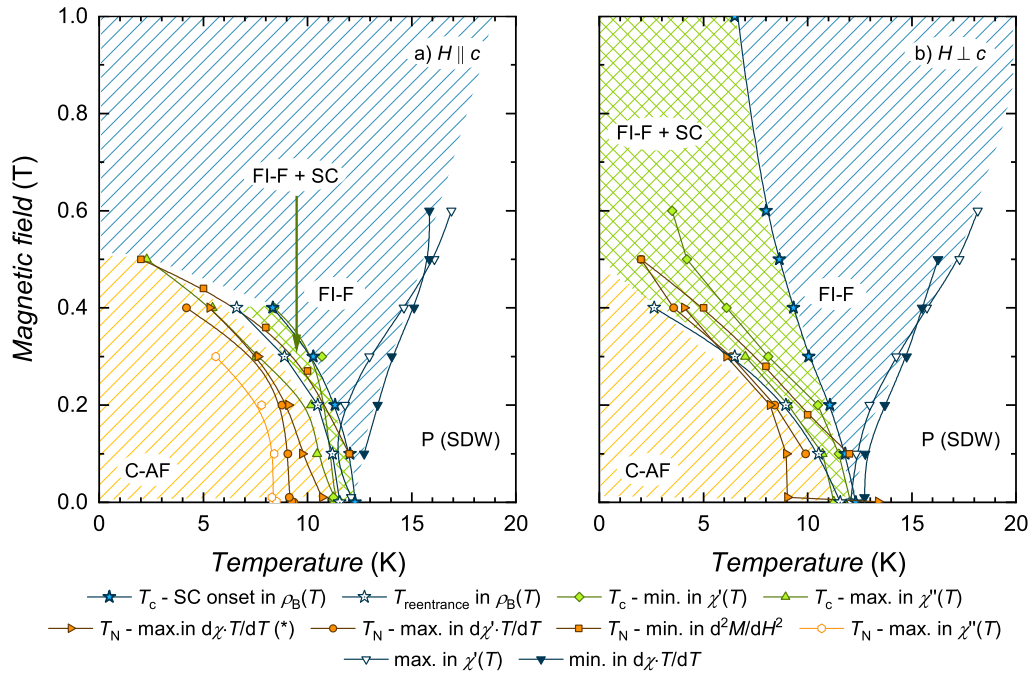


FIG. 11. Magnetic phase diagram of $\text{Eu}_{0.73}\text{Ca}_{0.27}(\text{Fe}_{0.87}\text{Co}_{0.13})_2\text{As}_2$ for fields applied (a) parallel and (b) perpendicular to the c axis.

arate broad maxima in $\chi'(T)$ are observed: one of them shifts to the lower temperatures and the other to higher temperatures with increasing magnetic field. The broad “peak” in $\chi''(T)$ shifts to the lower temperatures and its intensity decreases at higher magnetic fields.

Similar features were observed for fields applied perpendicular to the c axis, i.e., (i) a sharp peak in the $\chi''(T)$ is visible at zero magnetic field at $T_c = 12$ K and is shifted to lower temperatures with increasing magnetic field; (ii) there is also a wide maximum in $\chi'(T)$ at zero magnetic field that is divided into two separate maxima when the external magnetic field increases. However, there is no significant decrease of χ' , i.e., there is no dip in $\chi'(T)$, at temperatures at which the χ'' peak appears, as was observed for $H \parallel c$ measurements.

For both measurements—in parallel and perpendicular field—an additional broad maximum is observed in the real part of susceptibility, starting from around 12 K and shifting to higher temperatures with increasing magnetic field.

Comparing susceptibility measurements to the magnetoresistivity data, we associate the sharp peak in $\chi''(T)$ and the dip (or only change of slope) of $\chi'(T)$ with the appearance of superconductivity. The broad maximum starting at 12 K, and shifting to the lower temperatures with increasing magnetic field, can be explained by the antiferromagnetic transition while the maximum that shifts to higher temperatures is most likely associated with the formation of the ferromagnetic component—due to the reorientation of the Eu^{2+} magnetic moments as a result of applied magnetic field, which is consistent with the magnetization measurements.

Based on these results, transition temperatures were determined.

Using the Fisher’s method, transition temperature to the antiferromagnetic order T_N was determined from the real part of ac susceptibility. The $T_N(H)$ data points are summarized in

Fig. 11 as orange full circles. The T - H points corresponding to the maxima in $\chi''(T)$ associated to the antiferromagnetic and superconducting transitions are summarized in Fig. 11 as orange open circles and full green triangles, respectively.

The transition line in the T - H magnetic phase diagram between the paramagnetic (where the magnetic moments of Eu^{2+} are paramagnetic) and antiferromagnetic states—thus the H_{cr}^* field—was determined as the high temperature maximum in the $\chi'(T)$.

IV. DISCUSSION

A. Magnetic phase diagram

Based on the experimental results a magnetic phase diagram of $\text{Eu}_{0.73}\text{Ca}_{0.27}(\text{Fe}_{0.87}\text{Co}_{0.13})_2\text{As}_2$ was constructed and is presented in Fig. 11.

For this system several magnetic phases can be distinguished: paramagnetic, paramagnetic with SDW order of Fe^{2+} magnetic moments, superconducting, canted-antiferromagnetic (C-AF), and field induced ferromagnetic (FI-F) of Eu^{2+} magnetic moments. Below $T_{\text{SDW}} = 80$ K the system exhibits a SDW order of Fe^{2+} magnetic moments, therefore the system is truly paramagnetic only above this temperature and all other phases coexist with the SDW phase.

One should note that, although the field induced ferromagnetic state is present for fields applied parallel as well as for fields applied perpendicular to the crystallographic c axis, the microscopic order is remarkably different, i.e., for fields higher than H_{cr} (or H_{cr}^*) the magnetic moment of Eu^{2+} ions are aligned on the direction of the applied magnetic field—for $H \parallel c$ the magnetic moments are parallel to the c axis, and for $H \perp c$ the magnetic moments are perpendicular to the c axis.

B. Superconductivity

Although, as expected, by simultaneous Ca doping the T_N could be decreased and simultaneously, T_c increased compared to the $\text{Eu}(\text{Fe}_{0.81}\text{Co}_{0.19})_2\text{As}_2$; the zero-resistivity and diamagnetic signal are destroyed as soon as the Eu magnetic sublattice orders antiferromagnetically. This behavior is especially interesting when comparing presented results to the Co-doped systems with $0.075 < x(\text{Co}) < 0.2$, such as $\text{Eu}(\text{Fe}_{0.81}\text{Co}_{0.19})_2\text{As}_2$, in which superconductivity appeared below T_N , therefore in an already antiferromagnetically ordered state [23,24,32,33,36,51,52]. (It should be noted that in some papers the given compositions were based on the nominal Co concentrations, also EDX analysis is not the best tool for determining the concentration in case of Co and Fe compounds. It seems that the best way to determine Co concentration in the EuFe_2As_2 -based systems is by comparing the T_{SDW} values).

To explain why superconductivity can coexist with Eu magnetic order in some of the Eu-122 systems [excluding $\text{Eu}_{0.73}\text{Ca}_{0.27}(\text{Fe}_{0.87}\text{Co}_{0.13})_2\text{As}_2$], we extend the previously proposed interpretation [32,33].

It was proposed by Klemm *et al.* [53] that in layered superconductors the pairing between electrons (or holes) from different layers is minor. Therefore, such systems will be anisotropic. The investigated superconductors have layered structure, where the FeAs layers, responsible for superconductivity in these materials, are perpendicular to the c axis, i.e., are spread on the ab plane. The EuFe_2As_2 -based systems are anisotropic, i.e., for $\text{Eu}(\text{Fe}_{0.81}\text{Co}_{0.19})_2\text{As}_2$ the anisotropy ratio was estimated to equal 2.4 [32], while for $\text{Eu}_{0.73}\text{Ca}_{0.27}(\text{Fe}_{0.87}\text{Co}_{0.13})_2\text{As}_2$ the anisotropy ratio $\Gamma = \frac{H_{\parallel ab}}{H_{\parallel c}}$ is approximately 1.4 at $T = 8$ K (see the Supplemental Material [43] for more details).

Superconductivity can be destroyed as a result of a paramagnetic pair breaking effect (PPB effect) or an orbital pair breaking effect (OPB effect).

While the PPB effect depends only on the intensity of the magnetic field (the greater the field, the greater the pair breaking), the contribution of the OPB effect in layered superconductors with high spin-orbit scattering rate will also strongly depend on the direction of the magnetic field. In short, the OPB effect is not present when the magnetic field is parallel to the superconducting layers. On the other hand, when the field is applied perpendicular to the superconducting layers the OPB effect is maximal.

The Co-doped EuFe_2As_2 -based systems are layered superconductors with a high spin-orbit scattering rate, however due to the magnetic moment of Eu^{2+} even with no external magnetic field applied, the superconducting layers are exposed to a magnetic field. Since the magnetic moments are canted from the ab plane, there are two magnetic components parallel and perpendicular to the superconducting layers. Depending on the composition of the compound, the contribution of the components will be different.

When comparing $\text{Eu}_{0.73}\text{Ca}_{0.27}(\text{Fe}_{0.87}\text{Co}_{0.13})_2\text{As}_2$ and $\text{Eu}(\text{Fe}_{0.81}\text{Co}_{0.19})_2\text{As}_2$ [or other Eu-122 systems with $0.075 < x(\text{Co}) < 0.2$] one has to have in mind that the microscopic magnetic structure on the Eu sublattice is different for these two compounds. As shown by the Mössbauer spectroscopy

and neutron scattering, the angle between the magnetic moment of Eu and the c axis ϑ changes with Co doping [25,36]. Although both $\text{Eu}_{0.73}\text{Ca}_{0.27}(\text{Fe}_{0.87}\text{Co}_{0.13})_2\text{As}_2$ and $\text{Eu}(\text{Fe}_{0.81}\text{Co}_{0.19})_2\text{As}_2$ ground state is canted antiferromagnetic (C-AF), based on Mössbauer spectroscopy study, it is known that in zero-magnetic field the angle ϑ is bigger for the Co-only-doped compound [$\vartheta \in [44^\circ, 60^\circ]$] than for the Ca-and-Co-doped one with $\vartheta \approx 30^\circ$ [25,44,54]. In other words, in the ground state, the superconducting layers experience a perpendicularly applied magnetic field (due to the magnetic moment of Eu^{2+}), however it is bigger for the $\text{Eu}_{0.73}\text{Ca}_{0.27}(\text{Fe}_{0.87}\text{Co}_{0.13})_2\text{As}_2$ than in the case of the $\text{Eu}(\text{Fe}_{0.81}\text{Co}_{0.19})_2\text{As}_2$ compound. This is probably the reason why superconductivity at low temperatures is destroyed for the Ca-and-Co-doped compound while not for the Co-doped one.

By applying an external magnetic field the magnetic moments of Eu^{2+} can be “rotated” with the final form of a field induced ferromagnetic (FI-F) order. Here, again, one should note that the FI-F order is contrasting between the situations at which the field is applied parallel and perpendicular to the c axis. Consequently, when the field is applied perpendicular to the c axis the OPB effect is minimal, both because the external magnetic field and the magnetic moments of Eu^{2+} are parallel to the superconducting layers, and so superconductivity is mostly destroyed due to the PPB effect. On the contrary, the OPB effect is maximal when the field is parallel to the c axis, especially above H_{cr} , when also the magnetic moments of Eu^{2+} are perpendicular to the superconducting layers.

V. SUMMARY

We have investigated magnetic and electrical transport properties of the $\text{Eu}_{0.73}\text{Ca}_{0.27}(\text{Fe}_{0.87}\text{Co}_{0.13})_2\text{As}_2$ compound and compared its properties to similar members of the EuFe_2As_2 -based family. Depending on the temperature and magnetic field applied, $\text{Eu}_{0.73}\text{Ca}_{0.27}(\text{Fe}_{0.87}\text{Co}_{0.13})_2\text{As}_2$ undergoes multiple phase transitions. With decreasing the temperature we observe a transition from the (i) paramagnetic state to (ii) spin density wave order of Fe^{2+} followed by (iii) superconducting transition and (iv) canted-antiferromagnetic order of Eu^{2+} magnetic moments. With application of an external magnetic field the Eu^{2+} magnetic moment reorients and (v) field-induced ferromagnetic order can also be observed. For graphical presentation a magnetic phase diagram was constructed (see Fig. 11). Depending on the direction of applied external magnetic field, superconductivity can coexist with the Eu^{2+} magnetic moments order.

The parameters calculated from electrical transport data are comparable to those obtained for other Co-doped EuFe_2As_2 -based compounds.

By simultaneous Co and Ca doping we were able to obtain a compound with superconductivity appearing above the antiferromagnetic order of Eu^{2+} magnetic moments. However, a reentrance behavior was observed—instead of zero resistivity and diamagnetic signal down to the lowest temperatures. We show that this behavior is a result of simultaneous coincidence of few effects—the anisotropy expected for layered superconductors [53], the difference of contributions of orbital pair

breaking effect depending on the direction of the magnetic field in relation to the superconducting pairs in such systems

and the magnetic structure of the compound, which also depends on the external magnetic field.

- [1] Ø. Fischer and M. B. Maple (eds.), *Superconductivity in Ternary Compounds I*, Topics in Current Physics, Vol. 32 (Springer Berlin Heidelberg, Berlin, Heidelberg, 1982).
- [2] M. B. Maple and Ø. Fischer (eds.), *Superconductivity in Ternary Compounds II*, Topics in Current Physics, Vol. 34 (Springer Berlin Heidelberg, Berlin, Heidelberg, 1982).
- [3] A. Kołodziejczyk, B. V. B. Sarkissian, and B. R. Coles, Magnetism and superconductivity in a transition metal compound: Y_4Co_3 , *J. Phys. F: Met. Phys.* **10**, L333 (1980).
- [4] A. Kołodziejczyk and C. Sułkowski, Susceptibility, magnetisation and critical behaviour of a magnetic superconductor: Y_9Co_7 , *J. Phys. F: Met. Phys.* **15**, 1151 (1985).
- [5] K. Kadowaki, H. Van der Meulen, J. Klaasse, M. Van Sprang, J. Koster, L. Roeland, F. De Boer, Y. Huang, A. Menovsky, and J. Franse, Coexistence of magnetism and high- T_c superconductivity in $\text{GdBa}_2\text{Cu}_3\text{O}_7$, *Physica B+C* **145**, 260 (1987).
- [6] M. B. Maple, Interplay between superconductivity and magnetism, *Physica B* **215**, 110 (1995); L. Vinet and A. Zhedanov, *J. Phys. A: Math. Theor.* **44**, 085201 (2011).
- [7] J. W. Lynn, S. Skanthakumar, Q. Huang, S. K. Sinha, Z. Hossain, L. C. Gupta, R. Nagarajan, and C. Godart, Magnetic order and crystal structure in the superconducting $\text{RNi}_2\text{B}_2\text{C}$ materials, *Phys. Rev. B* **55**, 6584 (1997).
- [8] K. H. Müller and V. N. Narozhnyi, Interaction of superconductivity and magnetism in borocarbide superconductors, *Rep. Prog. Phys.* **64**, 943 (2001).
- [9] C. Noce, A. Vecchione, M. Cuoco, and A. Romano (eds.), *Ruthenate and Rutheno-Cuprate Materials*, Lecture Notes in Physics, Vol. 603 (Springer Berlin Heidelberg, Berlin, Heidelberg, 2002).
- [10] T. Nachtrab, C. Bernhard, C. Lin, D. Koelle, and R. Kleiner, The ruthenocuprates: Natural superconductor-ferromagnet multilayers, *C. R. Phys.* **7**, 68 (2006).
- [11] A. Lebed (ed.), *The Physics of Organic Superconductors and Conductors*, Springer Series in Materials Science, Vol. 110 (Springer Berlin Heidelberg, Berlin, Heidelberg, 2008).
- [12] C. Pfleiderer, Superconducting phases of f -electron compounds, *Rev. Mod. Phys.* **81**, 1551 (2009).
- [13] R. Niewa, L. Shlyk, and B. Blaschkowski, Rare-earth metal transition metal borocarbide and nitridoborate superconductors, *Z. Krist.* **226**, 352 (2011).
- [14] D. Aoki, F. Hardy, A. Miyake, V. Taufour, T. D. Matsuda, and J. Flouquet, Properties of ferromagnetic superconductors, *C. R. Phys.* **12**, 573 (2011).
- [15] G. Knebel, D. Aoki, and J. Flouquet, Antiferromagnetism and superconductivity in cerium based heavy-fermion compounds, *C. R. Phys.* **12**, 542 (2011).
- [16] Ł. Bochenek, K. Rogacki, A. Kołodziejczyk, and T. Cichorek, Y_9Co_7 : Evidence for local coexistence of superconductivity and itinerant ferromagnetism, *Phys. Rev. B* **91**, 235314 (2015).
- [17] M. Rotter, M. Tegel, and D. Johrendt, Superconductivity at 38 K in the Iron Arsenide $(\text{Ba}_{1-x}\text{K}_x)\text{Fe}_2\text{As}_2$, *Phys. Rev. Lett.* **101**, 107006 (2008).
- [18] G. Wu, H. Chen, T. Wu, Y. L. Xie, Y. J. Yan, R. H. Liu, X. F. Wang, J. J. Ying, and X. H. Chen, Different resistivity response to spin-density wave and superconductivity at 20 K in $\text{Ca}_{1-x}\text{Na}_x\text{Fe}_2\text{As}_2$, *J. Phys.: Condens. Matter* **20**, 422201 (2008).
- [19] H. Q. Yuan, J. Singleton, F. F. Balakirev, S. a. Baily, G. F. Chen, J. L. Luo, and N. L. Wang, Nearly isotropic superconductivity in $(\text{Ba,K})\text{Fe}_2\text{As}_2$, *Nature (London)* **457**, 565 (2009).
- [20] Y. He, T. Wu, G. Wu, Q. J. Zheng, Y. Z. Liu, H. Chen, J. J. Ying, R. H. Liu, X. F. Wang, Y. L. Xie, Y. J. Yan, J. K. Dong, S. Y. Li, and X. H. Chen, Evidence for competing magnetic and superconducting phases in superconducting $\text{Eu}_{1-x}\text{Sr}_x\text{Fe}_{2-y}\text{Co}_y\text{As}_2$ single crystals, *J. Phys.: Condens. Matter* **22**, 235701 (2010).
- [21] A. S. Sefat, R. Jin, M. A. McGuire, B. C. Sales, D. J. Singh, and D. Mandrus, Superconductivity at 22 K in Co-doped BaFe_2As_2 crystals, *Phys. Rev. Lett.* **101**, 117004 (2008).
- [22] S. Jiang, H. Xing, G. Xuan, Z. Ren, C. Wang, Z.-A. Xu, and G. Cao, Superconductivity and local-moment magnetism in $\text{Eu}(\text{Fe}_{0.89}\text{Co}_{0.11})_2\text{As}_2$, *Phys. Rev. B* **80**, 184514 (2009).
- [23] J. J. Ying, T. Wu, Q. J. Zheng, Y. He, G. Wu, Q. J. Li, Y. J. Yan, Y. L. Xie, R. H. Liu, X. F. Wang, and X. H. Chen, Electron spin resonance in $\text{EuFe}_{2-x}\text{Co}_x\text{As}_2$ single crystals, *Phys. Rev. B* **81**, 052503 (2010).
- [24] M. Matusiak, Z. Bukowski, and J. Karpinski, Doping dependence of the Nernst effect in $\text{Eu}(\text{Fe}_{1-x}\text{Co}_x)_2\text{As}_2$: Departure from Dirac-fermion physics, *Phys. Rev. B* **83**, 224505 (2011).
- [25] A. Błachowski, K. Ruebenbauer, J. Żukrowski, Z. Bukowski, K. Rogacki, P. J. W. Moll, and J. Karpinski, Interplay between magnetism and superconductivity in $\text{EuFe}_{2-x}\text{Co}_x\text{As}_2$ studied by ^{57}Fe and ^{151}Eu Mössbauer spectroscopy, *Phys. Rev. B* **84**, 174503 (2011).
- [26] L. Harnagea, S. Singh, G. Friemel, N. Leps, D. Bombor, M. Abdel-Hafiez, A. U. B. Wolter, C. Hess, R. Klingeler, G. Behr, S. Wurmehl, and B. Büchner, Phase diagram of the iron arsenide superconductors $\text{Ca}(\text{Fe}_{1-x}\text{Co}_x)_2\text{As}_2$ ($0 \leq x \leq 0.2$), *Phys. Rev. B* **83**, 094523 (2011).
- [27] M. Nicklas, M. Kumar, E. Lengyel, W. Schnelle, and A. Leithe-Jasper, Competition of local-moment ferromagnetism and superconductivity in Co-substituted EuFe_2As_2 , *J. Phys.: Conf. Ser.* **273**, 012101 (2011).
- [28] H.-A. Krug von Nidda, S. Kraus, S. Schaile, E. Dengler, N. Pascher, M. Hemmida, M. J. Eom, J. S. Kim, H. S. Jeevan, P. Gegenwart, J. Deisenhofer, and A. Loidl, Electron spin resonance in Eu-based iron pnictides, *Phys. Rev. B* **86**, 094411 (2012).
- [29] V. K. Anand, D. T. Adroja, A. Bhattacharyya, U. B. Paramanik, P. Manuel, A. D. Hillier, D. Khalyavin, and Z. Hossain, μSR and neutron diffraction investigations on the reentrant ferromagnetic superconductor $\text{Eu}(\text{Fe}_{0.86}\text{Ir}_{0.14})_2\text{As}_2$, *Phys. Rev. B* **91**, 094427 (2015).
- [30] Z. Ren, Q. Tao, S. Jiang, C. Feng, C. Wang, J. Dai, G. Cao, and Z. Xu, Superconductivity induced by phosphorus doping and its coexistence with ferromagnetism in $\text{EuFe}_2(\text{As}_{0.7}\text{P}_{0.3})_2$, *Phys. Rev. Lett.* **102**, 137002 (2009).

- [31] H. S. Jeevan, D. Kasinathan, H. Rosner, and P. Gegenwart, Interplay of antiferromagnetism, ferromagnetism, and superconductivity in $\text{EuFe}_2(\text{As}_{1-x}\text{P}_x)_2$ single crystals, *Phys. Rev. B* **83**, 054511 (2011).
- [32] V. H. Tran, Z. Bukowski, L. M. Tran, and A. J. Zaleski, The electronic phase diagrams of the $\text{Eu}(\text{Fe}_{0.81}\text{Co}_{0.19})_2\text{As}_2$ superconductor, *New J. Phys.* **14**, 073052 (2012).
- [33] V. H. Tran, T. A. Zaleski, Z. Bukowski, L. M. Tran, and A. J. Zaleski, Tuning superconductivity in $\text{Eu}(\text{Fe}_{0.81}\text{Co}_{0.19})_2\text{As}_2$ with magnetic fields, *Phys. Rev. B* **85**, 052502 (2012).
- [34] L. M. Tran, M. Babij, L. Korosec, T. Shang, Z. Bukowski, and T. Shiroka, Magnetic phase diagram of Ca-substituted EuFe_2As_2 , *Phys. Rev. B* **98**, 104412 (2018).
- [35] S. Zapf and M. Dressel, Europium-based iron pnictides: a unique laboratory for magnetism, superconductivity and structural effects, *Rep. Prog. Phys.* **80**, 016501 (2017).
- [36] W. T. Jin, Y. Xiao, Z. Bukowski, Y. Su, S. Nandi, A. P. Sazonov, M. Meven, O. Zaharko, S. Demirdis, K. Nemkovski, K. Schmalzl, L. M. Tran, Z. Guguchia, E. Feng, Z. Fu, and T. Brückel, Phase diagram of Eu magnetic ordering in Sn-flux-grown $\text{Eu}(\text{Fe}_{1-x}\text{Co}_x)_2\text{As}_2$ single crystals, *Phys. Rev. B* **94**, 184513 (2016).
- [37] A. Mitsuda, T. Matoba, F. Ishikawa, Y. Yamada, and H. Wada, Pressure-induced superconductivity in $\text{Eu}_{0.5}\text{Ca}_{0.5}\text{Fe}_2\text{As}_2$: Wide zero-resistivity region due to suppression of Eu magnetic order and chemical pressure, *J. Phys. Soc. Jpn.* **79**, 073704 (2010).
- [38] A. Mitsuda, T. Matoba, S. Seike, F. Ishikawa, Y. Yamada, and H. Wada, Effect of substitution of Ca^{2+} for Eu^{2+} on pressure-induced superconductivity in EuFe_2As_2 , *J. Phys. Soc. Jpn.* **80**, SA117 (2011).
- [39] A. Mitsuda, S. Seike, T. Matoba, H. Wada, F. Ishikawa, and Y. Yamada, Competition between Fe-based superconductivity and antiferromagnetism of Eu^{2+} in $\text{Eu}_{1-x}\text{Ca}_x\text{Fe}_2\text{As}_2$, *J. Phys.: Conf. Ser.* **273**, 012100 (2011).
- [40] L. Harnagea, R. Kumar, S. Singh, S. Wurmehl, A. U. B. Wolter, and B. Büchner, Evolution of the magnetic order of Fe and Eu sublattices in $\text{Eu}_{1-x}\text{Ca}_x\text{Fe}_2\text{As}_2$ ($0 \leq x \leq 1$) single crystals, *J. Phys.: Condens. Matter* **30**, 415601 (2018).
- [41] K. Shrestha, L. Z. Deng, K. Zhao, B. I. Jawdat, B. Lv, B. Lorenz, and C. W. Chu, Doping dependence and high-pressure studies on $\text{Eu}_x\text{Ca}_{1-x}\text{Fe}_2\text{As}_2$ ($0 \leq x \leq 1$), *Supercond. Sci. Technol.* **33**, 095010 (2020).
- [42] W. T. Jin, M. Meven, A. P. Sazonov, S. Demirdis, Y. Su, Y. Xiao, Z. Bukowski, S. Nandi, and T. Brückel, Spin reorientation of the Fe moments in $\text{Eu}_{0.5}\text{Ca}_{0.5}\text{Fe}_2\text{As}_2$: Evidence for strong interplay of Eu and Fe magnetism, *Phys. Rev. B* **99**, 140402(R) (2019).
- [43] See Supplemental Material at <http://link.aps.org/supplemental/10.1103/PhysRevB.109.014509> for more information about the Reentrant resistivity due to the interplay of superconductivity and magnetism in $\text{Eu}_{0.73}\text{Ca}_{0.27}(\text{Fe}_{0.87}\text{Co}_{0.13})_2\text{As}_2$.
- [44] K. Komędera, A. Błachowski, K. Ruebenbauer, J. Żukrowski, S. M. Dubiel, L. M. Tran, M. Babij, and Z. Bukowski, Mössbauer study of $\text{Eu}_{0.57}\text{Ca}_{0.43}\text{Fe}_2\text{As}_2$ and $\text{Eu}_{0.73}\text{Ca}_{0.27}(\text{Fe}_{0.87}\text{Co}_{0.13})_2\text{As}_2$: A comparison to ‘122’ iron-based superconductors parent compounds EuFe_2As_2 and CaFe_2As_2 , *J. Magn. Magn. Mater.* **457**, 1 (2018).
- [45] Z. Ren, Z. Zhu, S. Jiang, X. Xu, Q. Tao, C. Wang, C. Feng, G. Cao, and Z. Xu, Antiferromagnetic transition in EuFe_2As_2 : A possible parent compound for superconductors, *Phys. Rev. B* **78**, 052501 (2008).
- [46] J. Ballinger, L. E. Wenger, Y. K. Vohra, and A. S. Sefat, Magnetic properties of single crystal EuCo_2As_2 , *J. Appl. Phys.* **111**, 07E106 (2012).
- [47] S. Jiang, Y. Luo, Z. Ren, Z. Zhu, C. Wang, X. Xu, Q. Tao, G. Cao, and Z. Xu, Metamagnetic transition in EuFe_2As_2 single crystals, *New J. Phys.* **11**, 025007 (2009).
- [48] U. B. Paramanik, D. Das, R. Prasad, and Z. Hossain, Reentrant superconductivity in $\text{Eu}(\text{Fe}_{1-x}\text{Ir}_x)_2\text{As}_2$, *J. Phys.: Condens. Matter* **25**, 265701 (2013).
- [49] R. Hu, S. L. Bud’ko, W. E. Straszheim, and P. C. Canfield, Phase diagram of superconductivity and antiferromagnetism in single crystals of $\text{Sr}(\text{Fe}_{1-x}\text{Co}_x)_2\text{As}_2$ and $\text{Sr}_{1-y}\text{Eu}_y(\text{Fe}_{0.88}\text{Co}_{0.12})_2\text{As}_2$, *Phys. Rev. B* **83**, 094520 (2011).
- [50] M. E. Fisher, Relation between the specific heat and susceptibility of an antiferromagnet, *Philos. Mag.* **7**, 1731 (1962).
- [51] W. T. Jin, S. Nandi, Y. Xiao, Y. Su, O. Zaharko, Z. Guguchia, Z. Bukowski, S. Price, W. H. Jiao, G. H. Cao, and T. Brückel, Magnetic structure of superconducting $\text{Eu}(\text{Fe}_{0.82}\text{Co}_{0.18})_2\text{As}_2$ as revealed by single-crystal neutron diffraction, *Phys. Rev. B* **88**, 214516 (2013).
- [52] X. Chen, Z. Ren, H. Ding, and L. Liu, Cobalt-doping effects in single crystalline and polycrystalline $\text{EuFe}_{2-x}\text{Co}_x\text{As}_2$ compounds, *Sci. China Phys. Mech. Astron.* **53**, 1212 (2010).
- [53] R. Klemm, A. Luther, and M. Beasley, Theory of the upper critical field in layered superconductors, *Phys. Rev. B* **12**, 877 (1975).
- [54] L. M. Tran, *Investigation of the Coexistence of Superconductivity and Magnetism in Substituted EuFe_2As_2* (Imt, Wrocław, 2017).